Life Sciences 235 (2019) 116828

Contents lists available at ScienceDirect

Life Sciences

journal homepage: www.elsevier.com/locate/lifescie

Disturbance of mitochondrial dynamics and mitophagy in sepsis-induced acute kidney injury

Jian-xing Liu, Chen Yang, Wei-huang Zhang, Hong-yong Su, Ze-jian Liu, Qingjun Pan*, Hua-feng Liu*

Key Laboratory of Prevention and Management of Chronic Kidney Disease of Zhanjiang City, Affiliated Hospital of Guangdong Medical University, Zhanjiang, Guangdong 524001, China

ARTICLE INFO

Keywords:
Septic acute kidney injury
Mitophagy
Mitochondria
Apoptosis
Fission and fusion

ABSTRACT

Aims: The renal tubule cells require a large number of mitochondria to supply ATP due to their high-energy demand during reabsorption and secretion against chemical gradients and result in mitochondria susceptible to disorder and injury during stress conditions. Injured mitochondria are eventually degraded by mitophagy, and disturbances in mitophagy are associated with the pathogenesis of acute kidney injury (AKI) such as diabetic nephropathy and glomerulosclerosis. However, whether a disturbance in mitophagy has occurred and the role it plays in (SAKI) is still unclear. Therefore, the aim of this study was to investigate the key features of mitophagy and mitochondrial dynamics in sepsis-induced acute kidney injury (SAKI).

Main methods: In this study, a murine septic AKI model induced by cecal ligation and puncture (CLP) was built; mitophagy and mitochondrial dynamics were measured in mice kidney in different time point.

Key findings: The results showed that mitochondrial dynamics were characterized by fission/fusion aberrant, however more inclined to fission, and mitochondrial associated apoptosis was elevated over-time during SAKI. Furthermore, mitophagy was impaired in the later phase of SAKI, although elevated in early stage of SAKI. The results indicate that the underlying mechanisms of impaired mitophagy may associate with the cleavage of Parkin via caspases activated by NLRP3, at least partly.

Significance: It is conceivable that this selective autophagic process and quality control machinery was impaired, leading to the accumulation of damaged mitochondria, oxidative stress, and cell death. Therefore, a targeted approach, by enhancing mitophagy during SAKI, may be a promising therapeutic strategy.

1. Introduction

Sepsis is among the most common causes of acute kidney injury (AKI), accounting for approximately 50% of all AKI cases [1]. The mortality of patients who suffer from AKI with sepsis is 30–60%, which is approximately two-fold of that in patients without AKI [2,3]. While the pathogenesis of septic AKI (SAKI) has received attention in recent years, the mechanisms leading to AKI remain unclear and controversial [4,5]. Notably, disordered renal bioenergetics were found to play a pivotal role during SAKI [6], and a 70% decrease in ATP levels was responsible for approximately 30% of the deaths within 8 h in rats with lipopolysaccharide-induced endotoxic shock [7]. A previous study showed that depletion of bio-energy was associated with the incapacity of renal tubular epithelial cells to use available oxygen and changes in the mitochondrial structure under bacterial endotoxin simulation [8].

It has been confirmed that the mitochondrial structure and function under stress conditions were the main causes of impaired bio-energy and cellular oxygen utilization [9–12], and pivotal for trigging fragmentation of mitochondrial and mitochondrial-associated pro-apoptotic protein-mediated apoptosis [13,14]. Dysfunctional mitochondria can be degraded by selective autophagy called mitophagy that facilitates the turnover of damaged mitochondria by engulfing into “autophagosomes” for degradation. In recent years, the vital role of mitophagy has been found in multiple diseases, including but not limited to aging, neurodegenerative disorders, and kidney diseases [15–17], and insufficient or an overabundance in mitophagy will resulting in the accumulation of damaged mitochondria or the lack of intracellular substances during mitochondrial respiration, eventually resulting in mitochondrial homeostasis quality control and bio-energy metabolism disorders or cell death [18–20].

Although studies have shown that persistent inflammation or reactive oxygen species (ROS) result in accumulating damage to

* Corresponding authors.
E-mail addresses: pqj@gdmu.edu.cn (Q. Pan), hf-liu@263.net (H.-f. Liu).

https://doi.org/10.1016/j.lfs.2019.116828
Received 20 July 2019; Received in revised form 25 August 2019; Accepted 31 August 2019
Available online 31 August 2019
0024-3205/

mitochondria and cells, a decreased capacity to clear damaged mitochondria affects the progression of diabetic nephropathy and glomerulosclerosis. However, changes in mitochondrial dynamics and the degradation process of injured mitochondria in SAKI remain unclear. Therefore, in this study, a murine septic AKI model induced by cecal ligation and puncture (CLP) was used to investigate the key features of mitophagy and mitochondrial dynamics in SAKI.

2. Materials and methods

2.1. Mice

Sixty-six specific pathogen-free (SPF) male C57BL/6 mice, weighing 18.0–22.0 g (approximately 7–8 weeks of age), were purchased from Guangdong Medical Laboratory Animal Center (SCXK-(Guangdong) 2013-0002). The mice acclimated in individually ventilated cages in an SPF laboratory for 1 week prior to the experiments. The room was maintained at a temperature of 22 ± 2 °C, with 50 ± 10% relative humidity and a 12-hours light/dark cycle. Food and water were provided ad libitum. All animal experiments were approved by the Laboratory Animal Services Center at Guangdong Medical University (Zhanjiang, China) (SYXK-(Guangdong) 2015-0147) and performed according to the guidelines of Animal Welfare and Ethics of the Institutional Animal Care and Use Committee. All experiments were carried out in a specific pathogen-free animal lab.

2.2. Materials

The primers were synthesized by Sangon Biotech Co., Ltd. (Shanghai, China), and primer sequences are shown in Table 1. A Simply total RNA extraction kit was purchased from Hangzhou Bioer Technology Co., Ltd. (Hangzhou, China). The reverse transcription kit and Q-PCR kit were obtained from Takara (Shiga, Japan). Deadend ™ Fluorometric TUNEL system was purchased from Promega (Madison, WI). The Creatinine kit and Blood Urea Nitrogen kit were purchased from Nanjing Jiancheng Bioengineering Institute (Nanjing, China). The Cystatin C ELISA kit was purchased from Jiangsu Enzyme Industrial Co., Ltd. (Yancheng, China). Pink1 monoclonal antibody (#6946S), Parkin monoclonal antibody (#4211S), and Bax polyclonal antibody (2772S) were purchased from Cell Signaling Technology (Danvers, MA). PGC-1α polyclonal antibody (ab54481), OPA1 monoclonal antibody (ab157457), Drp1 monoclonal antibody (ab184247), NADPH oxidase 4 monoclonal antibody (ab133303), caspase 1 monoclonal antibody (ab179515), caspase 9 monoclonal antibody (ab202068), caspase 3 monoclonal antibody (ab184787), cleaved caspase3 monoclonal antibody (ab2302), LC3 polyclonal antibody (ab51520), and P62 monoclonal antibody (ab54616) were purchased from Abcam (Cambridge, UK). Cytochrome C monoclonal antibody (sc-13560) was purchased from Santa Cruz Biotechnology (Dallas, TX) and the NLRP3 polyclonal antibody (NBP177080) was purchased from Novus Biologicals (Littleton, CO). Bcl-2 polyclonal antibody (AB112), GAPDH monoclonal antibody (AF1186), horseradish peroxidase-goat anti-mouse (A0216), and horseradish peroxidase-goat anti-rabbit antibody (A0208) were purchased from Beyotime Biotechnology (Shanghai, China).

Table 1
Primer sequences.

Gene name	Forward	Reverse
PGC-1α	AGCCTCTTTGCCCAGATCTCTT	GGCAATCCGTCTTCATCCAC
OPA1	TACCACAGTCCGGAAGAACC	ATTCGCCAAAACAGGACCAC
Drp1	GCAACTGGAGAGGAATGCTG	CACAATCTAGCTGTTCTCGG
TOM 20	GCTAAGGAGAGAGCTGGGCTTT	TGGTCCACACCCTTCTCGTAGT
GAPDH	AACTTTGGCATTGTGGAAGG	ACACATTGGGGGTAGGAACA

Abbreviation: PGC-1α, peroxisome proliferator-activated receptor gamma coactivator-1 alpha; OPA1, mitochondrial dynamin-like GTPase; Drp1, dynamin-related protein 1; TOM20, translocase of outer mitochondrial membrane 20; GAPDH, glycolytic glyceraldehyde-3-phosphate dehydrogenase.

2.3. Preparation of septic acute kidney injury in mice

The mice that were subjected to CLP were randomly assigned to the following groups: 4 h, 8 h, 12 h, 18 h, and 24 h group (6 mice per group). The procedure was as described in the literature [21]. Briefly, the mice were anesthetized with pentobarbital sodium (50 mg per kg body weight, *i.p.*), and then placed onto Styrofoam pads on their backs. A midline longitudinal incision (approximately 1 cm) was made; the cecum was ligated 1 cm from the tip. Next, the cecum was punctured by single through-and-through puncture with 21-G needles midway between the ligation and tip, and a small amount of feces was extruded from both holes to ensure patency. The cecum was replaced into the abdominal cavity, followed by the closure of the abdominal musculature and skin. The mice were resuscitated by injecting pre-warmed normal saline (37 °C; 0.5 mL per mouse) subcutaneously. The mice in the control group ($n = 6$) underwent the same procedure but were neither ligated nor punctured. Mice were sacrificed at 4 h, 8 h, 12 h, 18 h, or 24 h after the CLP procedure, and the serum and kidneys were harvested for analysis.

2.4. Renal function evaluation

Creatinine and blood urea nitrogen levels were detected by the sarcosine oxidase method and urease method [22,23], respectively. Cystatin C levels in the serum were evaluated with an enzyme-linked immunosorbent assay kit according to the manufacturer's instructions.

2.5. Histopathology

Mouse kidneys were harvested, and the middle poles of the left kidney were fixed in 4% paraformaldehyde (pH = 7.4), dehydrated, embedded in paraffin, sectioned (thickness, 3 μm), and stained with Periodic Acid-Schiff stain. Kidney injury was scored according to the Paller scoring method [24] (dilatation or flatness of renal tubules: 1 point; brush border injury: 1 point, shedding of brush border: 2 points; cast: 2 points, detached or necrotic cells in the lumen of the tubule: 1 point) by two pathologists. The total score was the sum of all scores in the renal tubular lumen.

2.6. Total RNA extraction and RT-PCR

Kidney tissue was disrupted in liquid nitrogen, and total cellular RNA was extracted and converted to cDNA according to the manufacturer's instructions. cDNA was amplified using a Roche Lightcycler 480 (Basel, Switzerland). Polymerase chain reaction (PCR) was carried out under the following conditions: 95 °C, 30 s (1 cycle); 95 °C, 5 s, 60 °C, 20 s (40 cycles); 95 °C, 5 s, 60 °C, 60 s (1 cycle), and the relative expression of genes was normalized to that of GADPH.

2.7. Western blotting

The expression of PGC-1α, OPA1, Drp1, caspase 3, caspase 9, Bcl-2, Bax, Pink1, Parkin, LC3, and P62 in the kidney was determined by Western blotting. Briefly, the sample was lysed and clarified by centrifugation at 10,000 × *g* for 10 min at 4 °C. After denaturation, proteins were separated by sodium dodecyl sulfate-polyacrylamide gel electrophoresis, transferred to polyvinylidene difluoride membrane, blocked with 5% bovine serum albumin, and sequentially incubated with the primary antibodies, followed by the secondary antibody. The area and integrated optical density of the bands were analyzed using ImagePro Plus 6.0 software (Media Cybernetics, Rockville, MD).

2.8. TUNEL assay

Apoptosis was detected by the TdT-mediated dUTP nick-end labeling (TUNEL) method according to the Deadend ™ Fluorometric TUNEL system's instructions. Briefly, the sections were deparaffinized, rehydrated by graded alcohol washes, and fixed in 4% formaldehyde. The tissue was then treated with recombinant Terminal Deoxynucleotidyl Transferase enzyme to form a polymeric tail on apoptotic cells, and fluorescein was visualized using a Leica TCS SP5 confocal microscope (Wetzlar, Germany).

2.9. Immunohistochemistry and immunofluorescence

The serial section was deparaffinized, rehydrated, and incubated with 3% H_2O_2, followed by blocking in 5% bovine serum albumin. Cleaved caspase 3, NADPH oxidase 4, and NLRP3 were retrieved by citrate antigen retrieval solution, and caspase 1 was retrieved by a powerful antigen retrieval solution, then incubated with the appropriate primary antibodies. Meanwhile, homotypic negative controls were processed in parallel with the corresponding IgG species in the appropriate dilutions, followed by the secondary goat-anti-rabbit IgG antibody. Immunostaining with DAB was followed by hematoxylin counterstaining. For immunofluorescence analysis, the sections were incubated with LC3 and COX IV antibodies and secondary antibodies conjugated with Alexa Fluor to monitor mitophagy, and the homotypic negative control was processed in parallel. The sections were counterstained with 4,6-diamidino-2 phenylindole, and their fluorescence signals were visualized using a Leica TCS SP5 confocal microscope. For the statistical analyses of integral optical density or fluorescence intensity, 10 random fields (about 640 μm × 640 μm per section) of the renal cortex within each section of 6 experimental kidneys from each group were counted. The overlap coefficient, Pearson's correlation, and collocation fluorescent density of LC3-COX IV were analysis with Image J software (NIH, Bethesda, MD). Semi-quantitative analysis of immunohistochemistry or immunofluorescence was carried according to the software instructions. Briefly, the image is converted into an 8-bit grayscale image, then corrected optical density and applied to all images of the same antibody. Pixel was chosen as the unit of measurement, adjust the appropriate measurement threshold and applied to all images of the same antibody. And then the integrated density of entire image was counted. For fluorescence semi-quantitative analysis, the image was undergone black and white reversal after being converted into a grayscale image and the rest steps are the same.

2.10. Statistical analyses

The experiments shown are a summary of the data from at least three independent experiments (each with duplicates). The statistical analyses were performed using SPSS statistical software (SPSS 20.0, USA). Firstly, the normality of the data was tested, and the intergroup differences were evaluated by one-way analysis of variance or Dunnett's T3 depending on the data normality. The rank-sum test was used to identify pathological damage. Normally distributed continuous variables are expressed as means ± standard deviation, while abnormally distributed continuous variables are expressed as the median. Categorical variables are expressed as percentage. The results with *P*-values of ≤ 0.05 were considered as statistically significant.

3. Results

3.1. Pathological change and renal function in mice with CLP

Firstly, the morbidity of CLP with a 1 cm cecum ligation and puncture was verified ($n = 15$), with the time of death varying from 24 h to 108 h with 50% mortality (Fig. 1C). Thus, the longest time point was set to 24 h in the following experiments. In other experiments, mice were sacrificed in the respective time to assess whether SAKI occurred in mice with CLP via morphological and renal functions. The results showed that renal cast and detached cells were scattered in the renal tubular lumen together with vacuolar degeneration starting 4 h after CLP and increased over time. Additionally, TUNEL-positive cells were also found scattered in the renal tubular epithelium and increased over time (Fig. 1A and B). In addition, renal functions were detected by measuring creatinine, blood urea nitrogen, and cystatin C and the results showed that all increased significantly in CLP mice from 8 h after CLP (Fig. 1D–F), and remained stable until 24 h after CLP.

3.2. Mitochondrial-mediated apoptotic proteins in the kidneys of CLP mice

Mitochondrial-mediated apoptosis in the kidneys of CLP mice was measured by immunoblotting assays. The results showed that the levels of cytochrome C and the pro-apoptotic protein, Bax, were increased during the early phase of CLP and persisted until 24 h post-CLP; however, the expression level of Bcl-2 notably decreased at 12 h after CLP. Additionally, downstream events in apoptosis induced by the leakage of cytochrome *c*, caspase 9, and caspase 3 were also detected, indicating that the expression levels of these pro-apoptotic proteins significantly increased in the kidneys of CLP mice (Fig. 2).

3.3. Mitochondrial dynamics were aberrant in the kidneys of CLP mice

The expressions of genes associated with mitochondrial biosynthesis, fission, and fusion were detected by RT-PCR and Western blotting. The results showed that the mRNA expression of peroxisome proliferator-activated receptor-gamma coactivator-1 alpha (PGC-1α) dramatically decreased in the kidneys of CLP mice in a time-dependent manner; in addition, the expression of translocase of outer mitochondrial membrane 20 (TOM 20), which reflects the total amount of mitochondria, was also decreased from 12 to 24 h after CLP, indicating that mitochondria biosynthesis was inhibited in the kidneys after CLP. Additionally, the mRNA expression of Mitochondrial dynamin-like GTPase (OPA1), which mediates the fusion of mitochondria, decreased over time, while that of Dynamin-related protein 1 (Drp1), which mediates the fission of the outer membrane of mitochondria, was increased in the later phase after CLP, indicating that mitochondria fusion was inhibited and fission was enhanced. Moreover, the results of the immunoblotting also indicated that mitochondrial biosynthesis and fusion were inhibited, while fission increased in the kidneys of CLP mice, which characterized by decreased level of PGC-1α and OPA1 and an elevated level of Drp1 over the time (Fig. 3).

3.4. Mitophagy was impaired in the kidneys of CLP mice in the later phase

Immunoblotting and immunofluorescence assays were performed to assess mitophagy levels based on the co-localization of cytochrome *c* oxidase IV (COX IV) and autophagy marker light chain 3 (LC3). The results showed that mitophagy was elevated in the early phase (4–8 h) in the kidneys of mice with CLP, characterized by elevated levels of LC3 and increased co-localization of COX IV and LC3. However, the level of LC3 was decreased in the kidneys of CLP mice from 18 h to 24 h, and the co-localization of COX IV and LC3 also decreased (Fig. 4). Moreover, the results of the immunoblotting assays also showed similar results. The level of PTEN induced putative kinase 1 (Pink1) and Parkin RBR E3 ubiquitin protein ligase (Parkin), causing elevated levels in the kidneys of CLP mice in the range of 4 h to 8 h after CLP, then decreasing from 18 h to 24 h. A similar trend was found in the expression level of LC3. In addition, the level of sequestosome 1 (P62) increased in the kidneys from 18 h to 24 h after CLP (Fig. 5).

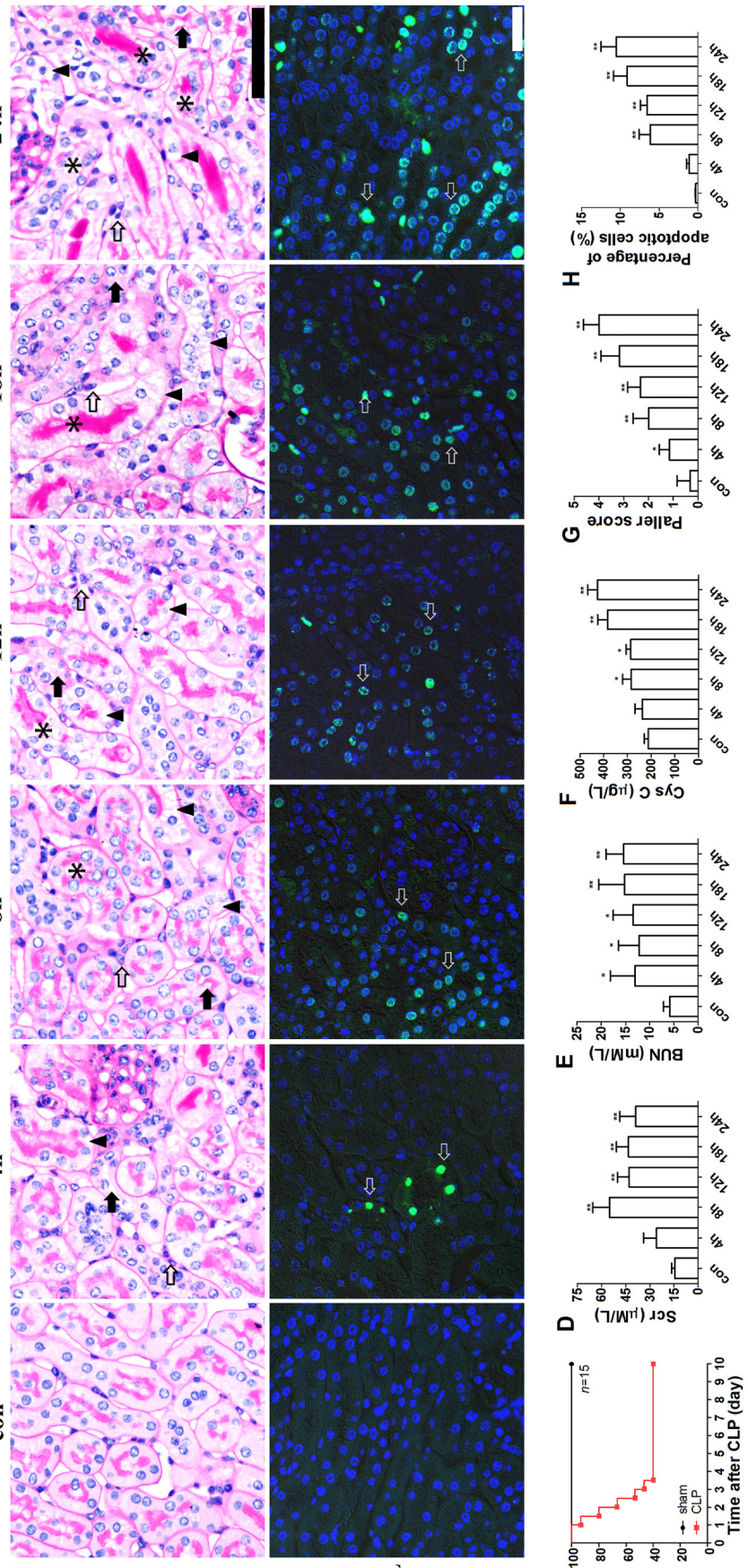

Fig. 1. Morphological and renal function in mice with CLP ($n = 6$). Mice were subjected to CLP and sacrificed at different times; pathological changes and renal function were evaluated. Representative images of PAS-stained kidney sections (white arrow: infiltration, asterisks: cast, arrowhead: vacuolization, arrow: loss of brush border; ×400) (A), TUNEL staining (green fluorescent spots, ×630) (B), bar = 50 μm. Survival of mice subjected to CLP with 1-cm cecum (C, $n = 15$), Serum creatinine (D), blood urea nitrogen (E), cystatin c (F), quantification of tubular injury (G), and percentage of TUNEL-positive cells (H). $^{*}P < 0.05$, $^{**}P < 0.01$ compared to control mice. (For interpretation of the references to color in this figure legend, the reader is referred to the web version of this article.)

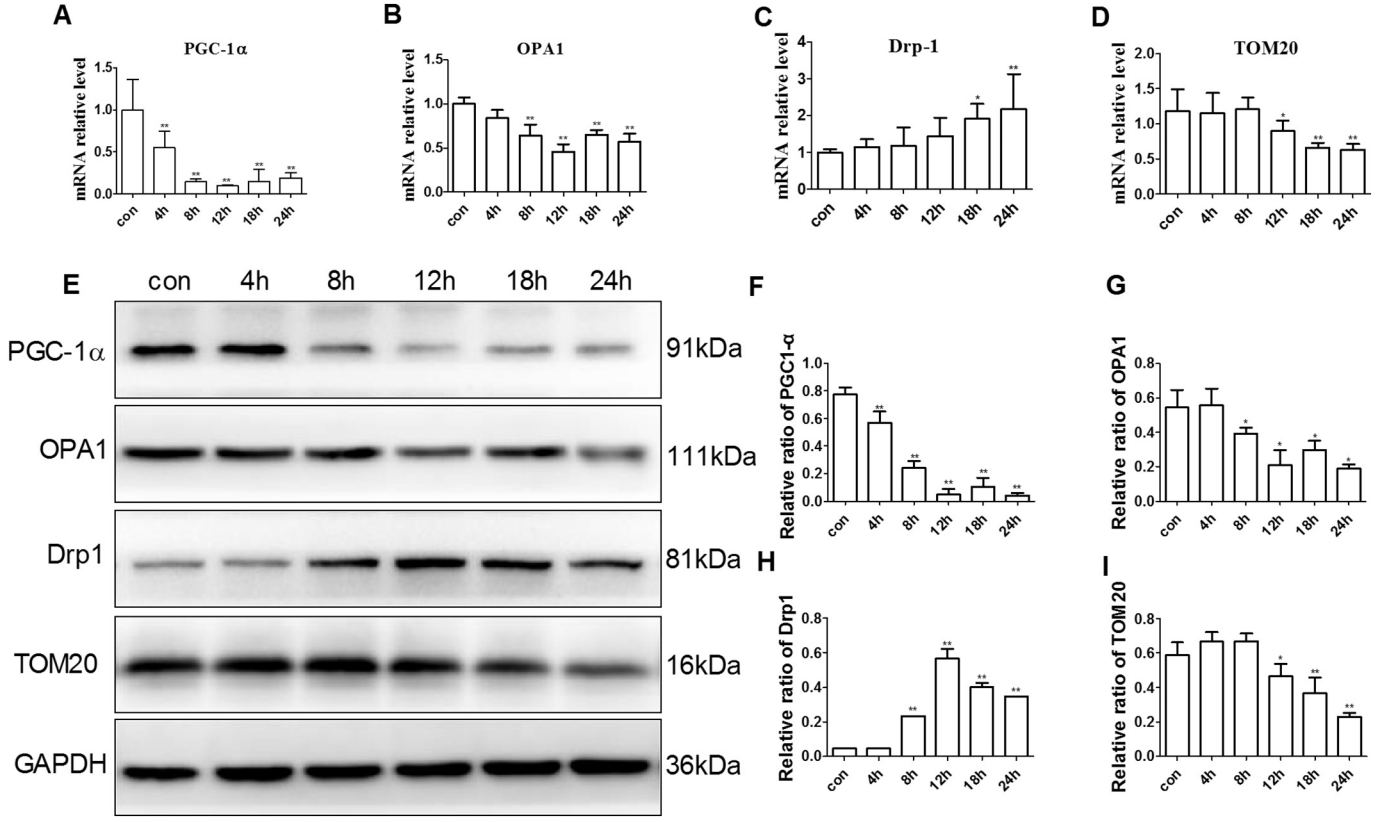

Fig. 2. Levels of mitochondria-associated apoptosis in the kidneys of CLP mice ($n = 6$). The levels of mitochondria-associated apoptotic proteins were analyzed by Western blotting at different times after CLP. Levels of Cytochrome c (1:1000), Bcl-2 (1:1000), Bax (1:2000), caspase9 (1:1000), and caspase3 (1:1000) detected by Western blotting (A), and quantified from triplicate experiments (B–G). $^{*}P < 0.05$, $^{**}P < 0.01$ compared to control mice. Cyt c: Cytochrome c, Bcl-2: B-cell lymphoma-2, Bax: Bcl-2 associated X protein.

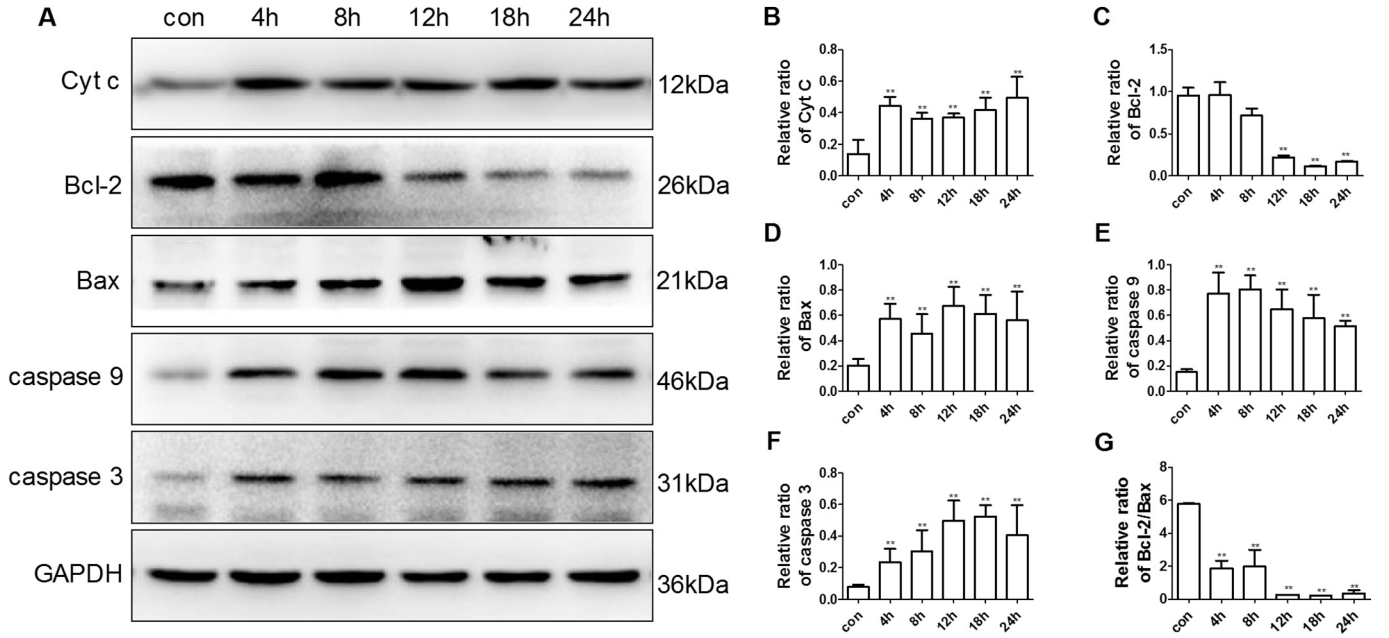

Fig. 3. Disturbance of mitochondria dynamics in the kidneys of CLP mice ($n = 6$). The dynamics of mitochondria in the kidney was analysis by RT-PCR and Western blotting at different times after CLP. The mRNA levels of PGC-1α, OPA-1, Drp-1, and TOM20 (A–D). Blotting images of PGC-1α (1:1000), OPA-1 (1:1000), Drp-1 (1:2000) and TOM20 (1:2000) (E), and quantification of triplicate experiments (F–I). $^{*}P < 0.05$, $^{**}P < 0.01$ compared to control mice. PGC-1α: peroxisome proliferator-activated receptor-gamma coactivator-1 alpha, OPA1: mitochondrial dynamin-like GTPase, Drp1: dynamin-related protein 1, TOM20: translocase of outer mitochondrial membrane 20, GAPDH: glycolytic glyceraldehyde-3-phosphate dehydrogenase.

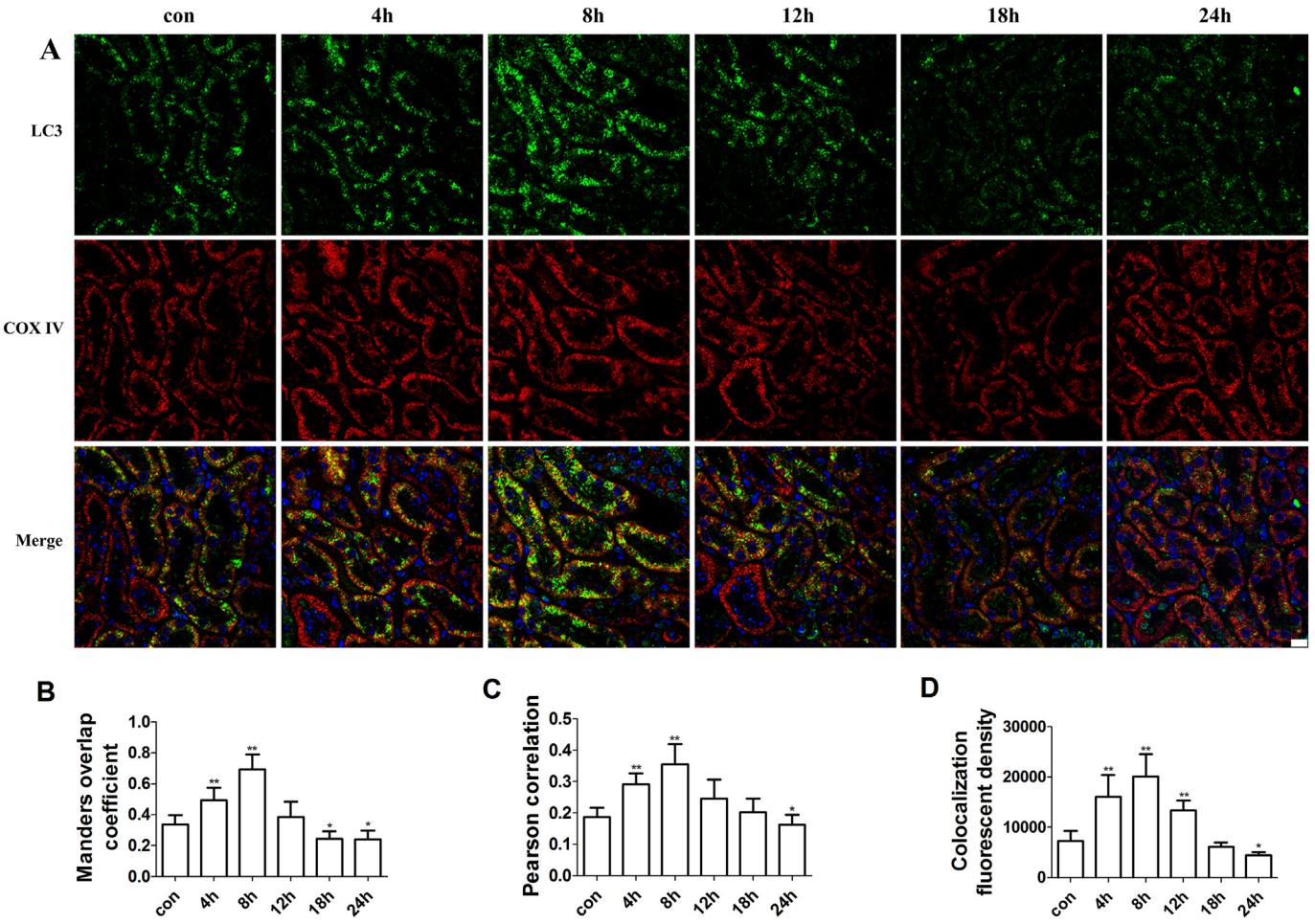

Fig. 4. Mitophagy was impaired in the kidneys of CLP mice in the later phase ($n = 6$). Paraffin sections were stained with anti-LC3 (1:300, green) and anti-COX IV (1:400, red) antibodies to reflect mitophagy by immunofluorescence at different times after CLP. Mitophagy levels were analyzed by confocal microscopy, and co-localization of LC3-COX IV was analyzed with Image J software. Representative images of mitophagy (A), overlap coefficient of LC3-COX IV (B), Pearson's correlation (C), and collocation fluorescent density (D). Bar = 25 μm. $^{*}P < 0.05$, $^{**}P < 0.01$ compared to control mice. COX IV: cytochrome c oxidase IV, LC3: autophagy marker light chain 3. (For interpretation of the references to color in this figure legend, the reader is referred to the web version of this article.)

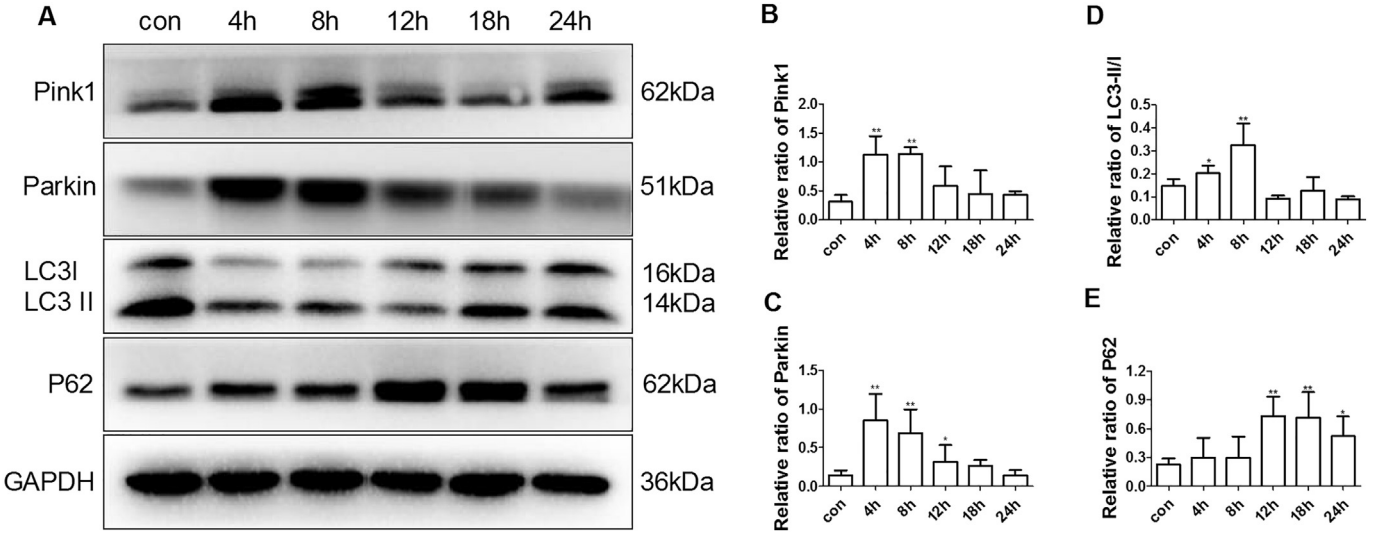

Fig. 5. Levels of mitophagy-associated proteins in CLP mice kidney ($n = 6$). The blotting images of Pink1 (1:1000), Parkin (1:1000), LC3 (1:1000) and P62 (1:1000) (A), and the quantification of triplicate experiments (B–E) at different times in kidneys of mice subjected to CLP. $^{*}P < 0.05$, $^{**}P < 0.01$ compared to control mice. Pink1: PTEN induced putative kinase 1, Parkin: Parkin RBR E3 ubiquitin protein ligase, P62: sequestosome 1.

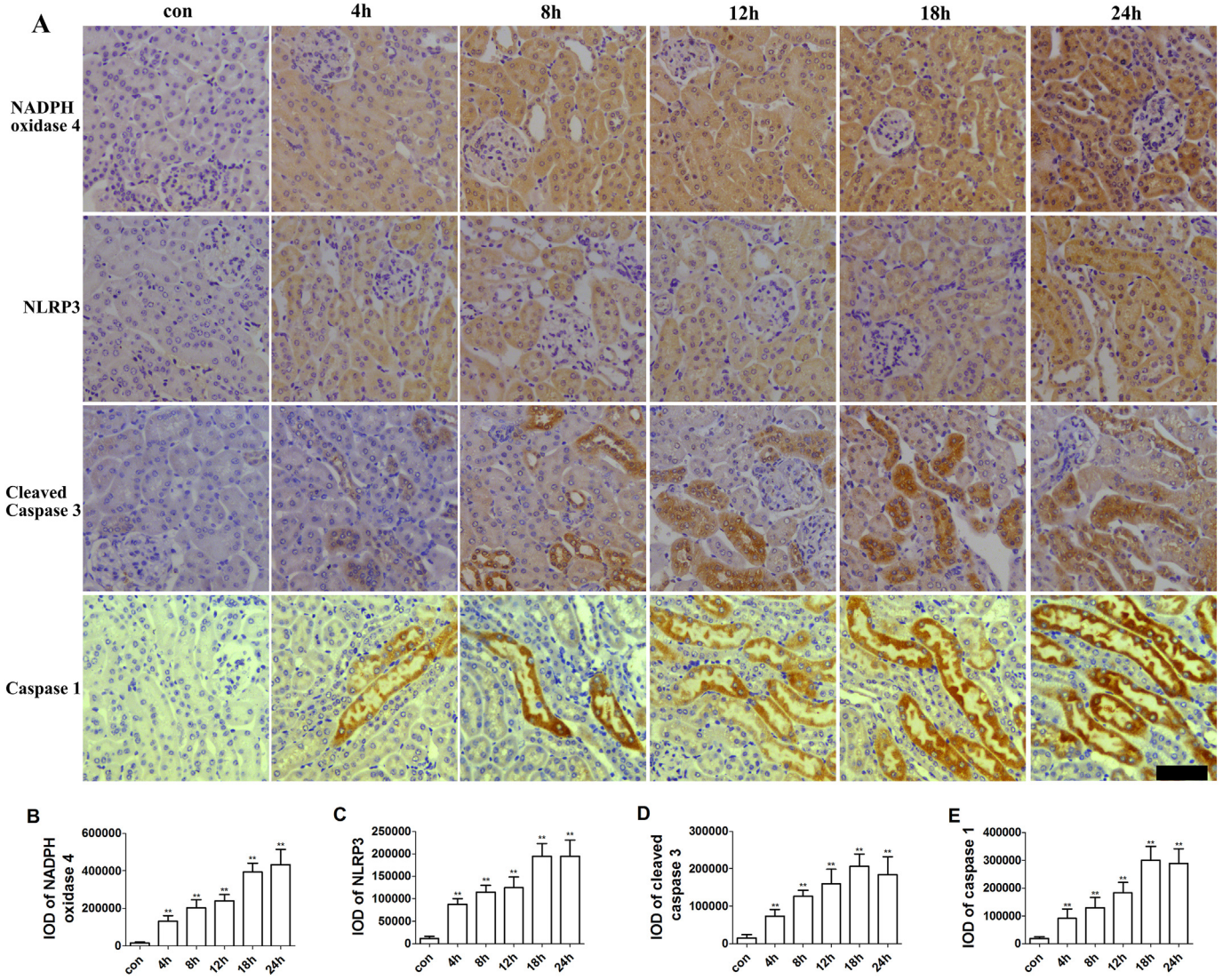

Fig. 6. NADPH oxidase 4, NLRP3, and cleaved caspase-3 expression in CLP-induced AKI ($n = 6$). The levels of NADPH oxidase 4 (1:200), NLRP3 (1:200), cleaved caspase-3 (1:300), and caspase-1 (1:300) (brown, ×400) were analyzed by immunohistochemistry at different times after CLP (A), bar = 50 μm. Quantification of NLRP3 and active caspase-3 (B–C). $^{*}P < 0.05$, $^{**}P < 0.01$ compared to control mice. NLRP3: NLR family pyrin domain containing 3. (For interpretation of the references to color in this figure legend, the reader is referred to the web version of this article.)

3.5. Inflammasomes, which mediated Parkin cleavage, were activated in the later phase of CLP

It has been confirmed that inflammation and mitophagy regulate each other, especially by the activation of the NLR family pyrin domain containing 3 (NLRP3) and stress-triggered apoptosis. The activation of NLRP3 could promote Parkin cleavage by activating the expression of caspase 1, caspase 3, and caspase 8, and subsequently inhibiting mitophagy. Thus, the levels of NLRP3 and caspases were detected by immunohistochemistry analysis due to the impaired mitophagy that occurred in the later phase of CLP. The results showed that the levels of NADPH oxidase 4 and NLRP3 were increased in the kidneys of CLP mice and increased over time. The caspases, such as caspase 1 and cleaved caspase 3 also increased over time in a similar trend, especially during 18 h to 24 h after CLP (Fig. 6).

4. Discussion

In the present study, we found that mitophagy was elevated in the earlier stage of SAKI; however, this protective process was impaired and accompanied by decreased levels of Pink1 and Parkin. Meanwhile, mitochondrial fission/fission balance was skewed to favor fission in the later stage of SAKI. In addition, the levels of NLRP3 and caspases family proteins dramatically increased in the later phase of SAKI.

The high energy supplement for filtration and reabsorption in the kidneys heavily relies on mitochondrial structure integrity and a highly oxidative phosphorylation turnover in the mitochondrial respiratory chain, and the morphology of the mitochondria plays a pivotal role in the decreased ATP levels and cell injury. Growing research showed that mitochondria could undergo various changes from mitochondrial permeability, decrease in the mitochondrial membrane potential to swelling and cristae disruption during stress [9,12,25]. These damages to the mitochondria trigger the release of apoptogenic factors, such as cytochrome *c*, and growing research has shown that the leakage of cytochrome *c* and mitochondrial damage were one of the earliest events during SAKI. The release of cytochrome *c* into the extracellular space increased in experimental and clinical AKI and correlated inversely with mitochondrial morphology and cell survival. Furthermore, the addition of exogenous cytochrome *c* to cultures induced cell apoptosis in vitro [26]. Moreover, other research showed that apoptosis induced by the release of cytochrome *c* is initially through the accumulation of Bax in the mitochondria by permeabilizing the mitochondrial outer

membrane, and thereby promoting the release of cytochrome *c* [12,27], and consequent activation of caspase 9 by binding to Apaf-1 in the cytosol, leading to the activation of the caspase cascade and apoptosis. Importantly, Bcl-2, as a regulator of permeabilization proteins, also plays a critical role in controlling the outer membrane integrity. Increased levels of Bax, accompanied by decreased Bcl-2 levels, were found in ischemic and endotoxin-induced AKI, while the knockout of Bax in kidneys reduced the release of cytochrome *c* and decreased apoptosis [28]. The release of mtDNA by damaged mitochondria also trigger the NLRP3-caspase-mediated apoptosis [29–31].

Furthermore, the accumulation of damaged mitochondria impacts the mitochondria fusion/fission balance that is a necessary process in maintaining the formation and function of mitochondria [32,33]. The fusion/fission of mitochondria is a precise process that involves regulation by multiple proteins and responding to various cellular signaling or stress to maintain mitochondrial quality control. A mitochondrion fusion relies on guanosine triphosphatases, mitofusin1, and mitofusion2 at the mitochondrial outer membrane and OPA1 on the inner membrane, whereas fission relies on Drp1 translocation into mitochondria to initiate fission by forming a spiral constriction ring with local receptors such as Fis1 on the outer membrane [10,34,35]. Importantly, these two opposite processes are necessary to avoid cell death during times of stress [36–38]. Studies have shown that the fusion/fission of mitochondria is based on the mitochondrial membrane potential; the fusion of functionally impaired mitochondrial (lower membrane potential) was suppressed, while fission was increased in AKI. In addition, decreased fusion or increased fission-induced cell death could be improved by the overexpression of OPA1, the blockade of Drp1, or through the use of the fission inhibitor, Mdivi-1 [32,33].

In addition to mitochondrial fusion/fission, degradation of damaged mitochondria is also an important process in maintaining mitochondrial homeostasis and quality control. In general, impaired mitochondria accompanied by a lower membrane potential usually skewed towards fission and could be degraded by mitophagy [39]. The degradation of Pink1 was suppressed in damaged mitochondria and resulted in the accumulation of Pink1 in the mitochondrial outer membrane [40,41], followed by recruitment of Parkin and ubiquitination of Mfn1 and Mfn2 to initiating mitophagy [42]. Mitophagy, as an evolutionarily conserved cellular process, plays an important role in maintaining the number of mitochondria and energy metabolism by clearing dysfunctional or redundant mitochondria, as well as preventing excessive ROS accumulation, inhibiting activation inflammation, and preventing apoptosis [15,43–46]. Moreover, there are several studies that show that the pathogenesis of several types of AKI is associated with impaired mitophagy, and the autophagy was also suppressed in CLP-induced AKI. However, the mechanism of this impaired mitophagy was partially revealed demonstrating that the accumulation of Parkin on the mitochondrial outer membrane could be degraded by the activation of NLRP3 and caspases family proteins, such as caspase-1, caspase-3, and caspase-8 [47,48]. Coincidentally, these proteins were increased in endotoxin-induced tissue damage. Interestingly, there appears to be a delicate balance between NLRP3, caspases, and mitophagy. It has been confirmed that the activation of mitophagy facilitates decreasing levels of NLRP3 and the caspases cascade [49], while activation of NLRP3 and the caspase family of proteins, such caspase-1, caspase-3, and caspase-8, inhibit mitophagy, and consequently aggravate inflammation and cell damage.

5. Conclusion

In conclusion, our results indicating that impaired mitophagy and aberrant mitochondrial dynamics contribute to renal tubular dysfunction in the later phase of septic AKI. Here, we hypothesized that in the early stage of sepsis, injured mitochondria could be effectively degraded by mitophagy. However, as injured mitochondria accumulate, the protective effects are overwhelmed, and the underlying mechanism of impaired mitophagy in the later phase of septic AKI was associated with the activation of NLRP3-caspases-mediated proteolytic cleavage of Parkin (Graphical Abstract).

Declaration of competing interest

The authors have no financial conflicts of interest.

Acknowledgments

This work was supported by the National Natural Science Foundation of China [grant number 81670654].

References

[1] S.M. Bagshaw, et al., Acute kidney injury in septic shock: clinical outcomes and impact of duration of hypotension prior to initiation of antimicrobial therapy, Intensive Care Med. 35 (5) (2008) 871–881.
[2] H. Shinjo, et al., Comparison of kidney disease: improving global outcomes and acute kidney injury network criteria for assessing patients in intensive care units, Clin. Exp. Nephrol. 18 (5) (2013) 737–745.
[3] Y. Fang, et al., Acute kidney injury in a Chinese hospitalized population, Blood Purif. 30 (2) (2010) 120–126.
[4] F. Fani, et al., Recent advances in the pathogenetic mechanisms of sepsis-associated acute kidney injury, J. Nephrol. 31 (3) (2017) 351–359.
[5] H. Gomez, et al., A unified theory of sepsis-induced acute kidney injury, Shock 41 (1) (2014) 3–11.
[6] R. Yang, et al., Energy and oxygen metabolism disorder during septic acute kidney injury, Kidney Blood Press. Res. 39 (4) (2014) 240–251.
[7] J.C. Duvigneau, et al., A novel endotoxin-induced pathway: upregulation of heme oxygenase 1, accumulation of free iron and free iron-mediated mitochondrial dysfunction, Lab. Investig. 88 (1) (2007) 70–77.
[8] C. Quoilin, et al., Endotoxin-induced basal respiration alterations of renal HK-2 cells: a sign of pathologic metabolism down-regulation, Biochem. Biophys. Res. Commun. 423 (2) (2012) 350–354.
[9] J.A. Funk, et al., Persistent disruption of mitochondrial homeostasis after acute kidney injury, Am. J. Physiol. Renal Physiol. 302 (2012) F853–F864.
[10] R.J. Youle, et al., Mitochondrial fission, fusion, and stress, SCIENCE 337 (2012) 1062–1065.
[11] J.R. Friedman, J. Nunnari, Mitochondrial form and function, Nature 505 (7483) (2014) 335–343.
[12] S.-G.C. Craig Brooks, C.-Y. Wang, T. Yang, Z. Dong, Fragmented mitochondria are sensitized to Bax insertion and activation during apoptosis, Am. J. Physiol. Cell Physiol. 300 (2011) C447–C455.
[13] A. Rimessi, et al., Mitochondrial reactive oxygen species and inflammation: molecular mechanisms, diseases and promising therapies, Int. J. Biochem. Cell Biol. 81 (2016) 281–293.
[14] H.K. Eltzschig, M.V. Sitkovsky, S.C. Robson, Purinergic signaling during inflammation, N. Engl. J. Med. 367 (24) (2012) 2322–2333.
[15] J.M.T. Hyttinen, et al., Mitochondrial quality control in AMD: does mitophagy play a pivotal role? Cell. Mol. Life Sci. 75 (16) (2018) 2991–3008.
[16] E.F. Fang, et al., Mitophagy inhibits amyloid-β and tau pathology and reverses cognitive deficits in models of Alzheimer's disease, Nat. Neurosci. 22 (3) (2019) 401–412.
[17] G.C. Higgins, M. C., Mitochondrial dysfunction and mitophagy: the beginning and end to diabetic nephropathy? Br. J. Pharmacol. 171 (8) (2014) 1917–1942.
[18] T. Kawakami, et al., Deficient autophagy results in mitochondrial dysfunction and FSGS, J. Am. Soc. Nephrol. 26 (5) (2015) 1040–1052.
[19] T. Namba, et al., Autophagic clearance of mitochondria in the kidney copes with metabolic acidosis, J. Am. Soc. Nephrol. 25 (10) (2014) 2254–2266.
[20] D.A. Kubli, A.B. Gustafsson, Mitochondria and mitophagy: the yin and yang of cell death control, Circ. Res. 111 (9) (2012) 1208–1221.
[21] D. Rittirsch, et al., Immunodesign of experimental sepsis by cecal ligation and puncture, Nat. Protoc. 4 (1) (2009) 31–36.
[22] H. Talke S.G., Enzymatic urea determination in the blood and serum in the Warburg optical test, Klin. Wochenschr. 43 (1965) 174–175.
[23] A.L. Chasson, H.J. Grady, M.A. Stanley, Determination of creatinine by means of automatic chemical analysis, Tech Bull Regist Med Technol 30 (1960) 207–212.
[24] M.S. Paller, T.V. Neumann, Reactive oxygen species and rat renal epithelial cells during hypoxia and reoxygenation, Kidney Int. 40 (6) (1991) 1041–1049.
[25] S.M. Parikh, et al., Mitochondrial function and disturbances in the septic kidney, Semin. Nephrol. 35 (1) (2015) 108–119.
[26] R. Codina, et al., Cytochrome c-induced lymphocyte death from the outside in: inhibition by serum leucine-rich alpha-2-glycoprotein-1, Apoptosis 15 (2) (2010) 139–152.
[27] C. Sheridan, et al., Bax- or Bak-induced mitochondrial fission can be uncoupled from cytochrome c release, Mol. Cell 31 (4) (2008) 570–585.
[28] Q. Wei, et al., Bax and Bak have critical roles in ischemic acute kidney injury in global and proximal tubule–specific knockout mouse models, Kidney Int. 84 (1) (2013) 138–148.
[29] R. van Bruggen, et al., Human NLRP3 inflammasome activation is Nox1-4

independent, Blood 115 (26) (2010) 5398–5400.
[30] M.J. Kong, et al., Mitochondrial NADP+-dependent isocitrate dehydrogenase deficiency increases cisplatin-induced oxidative damage in the kidney tubule cells, Cell Death Dis. 9 (5) (2018).
[31] W. Ding, et al., Mitochondria-targeted antioxidant mito-tempo protects against aldosterone-induced renal injury in vivo, Cell. Physiol. Biochem. 44 (2) (2017) 741–750.
[32] D. Perdiz, et al., Stress-induced hyperacetylation of microtubule enhances mitochondrial fission and modulates the phosphorylation of Drp1 at 616 Ser, Cell. Signal. 39 (2017) 32–43.
[33] I. Garcia, et al., Oxidative insults disrupt OPA1-mediated mitochondrial dynamics in cultured mammalian cells, Redox Rep. 23 (1) (2018) 160–167.
[34] B. Westermann, Bioenergetic role of mitochondrial fusion and fission, Biochim. Biophys. Acta Bioenerg. 1817 (10) (2012) 1833–1838.
[35] M. Zhan, et al., Mitochondrial dynamics: regulatory mechanisms and emerging role in renal pathophysiology, Kidney Int. 83 (4) (2013) 568–581.
[36] Q.D. Sung-Gyu Cho, Shuang Huang, Zheng Dong, Drp1 dephosphorylation in ATP depletion-induced mitochondrial injury and tubular cell apoptosis, Am. J. Physiol. Renal Physiol. 299 (2010) F199–F206.
[37] Y.H. Xiao Xiao, Pedro M. Quirós, Qingqing Wei, Carlos López-Otín, Zheng Dong, OMA1 mediates OPA1 proteolysis and mitochondrial fragmentation in experimental models of ischemic kidney injury, Am. J. Physiol. Renal Physiol. 306 (2014) F1318–F1326.
[38] S.M. Parikh, Therapeutic targeting of the mitochondrial dysfunction in septic acute kidney injury, Curr. Opin. Crit. Care 19 (6) (2013) 554–559.
[39] E. Deas, et al., PINK1 cleavage at position A103 by the mitochondrial protease PARL, Hum. Mol. Genet. 20 (5) (2011) 867–879.
[40] A.J. Whitworth, et al., Oxidative stress and regulation of pink1 in zebrafish (Danio rerio), PLoS One 8 (11) (2013) e81851.
[41] S.M. Jin, R.J. Youle, The accumulation of misfolded proteins in the mitochondrial matrix is sensed by PINK1 to induce PARK2/Parkin-mediated mitophagy of polarized mitochondria, Autophagy 9 (11) (2014) 1750–1757.
[42] S. Lee, C. Zhang, X. Liu, Role of glucose metabolism and ATP in maintaining PINK1 levels during Parkin-mediated mitochondrial damage responses, J. Biol. Chem. 290 (2) (2015) 904–917.
[43] Naeem K. Patil, N. P, Lee Ann MacMillan-Crow, Philip R. Mayeux, Inactivation of renal mitochondrial respiratory complexes and manganese superoxide dismutase during sepsis: mitochondria-targeted antioxidant mitigates injury, Am. J. Physiol. Renal Physiol. 306 (2014) F734–F743.
[44] C. Quoilin, et al., Evidence of oxidative stress and mitochondrial respiratory chain dysfunction in an in vitro model of sepsis-induced kidney injury, Biochim. Biophys. Acta Bioenerg. 1837 (10) (2014) 1790–1800.
[45] E. Pathak, L.A. MacMillan-Crow, P.R. Mayeux, Role of mitochondrial oxidants in an in vitro model of sepsis-induced renal injury, J. Pharmacol. Exp. Ther. 340 (1) (2011) 192–201.
[46] A. Picca, et al., Fueling inflamm-aging through mitochondrial dysfunction: mechanisms and molecular targets, Int. J. Mol. Sci. 18 (5) (2017) 933.
[47] Yu, H. Jiujiu, Tomohiko Murakami, Hai Hoang, Lori Broderick, Hal M. Hoffman, Tiffany Horng, Inflammasome activation leads to caspase-1-dependent mitochondrial damage and block of mitophagy, PNAS 111 (43) (2014) 15514–15519.
[48] S. Kahns, et al., Caspase-1 and caspase-8 cleave and inactivate cellular Parkin, J. Biol. Chem. 278 (26) (2003) 23376–23380.
[49] Y. Xu, W.J., W. Xu, F. Ding, W. Ding, Prohibitin 2-mediated mitophagy attenuates renal tubular epithelial cells injury by regulating mitochondrial dysfunction and NLRP3 inflammasome activation, Am. J. Physiol. Renal Physiol. 316 (2) (2019) F396–F407.